Structure and elasticity of polyurethane networks based on poly(butadiene) diol, 4,4′-diphenylmethane diisocyanate and poly(oxypropylene) triol

Ivan Krakovský*, Josef Pleštil, Michal Ilavský and Karel Dušek
Institute of Macromolecular Chemistry, 162 06 Prague 6, Czech and Slovak Federal Republic
(Received 24 August 1992; revised 23 December 1992)

Relations between structure and equilibrium mechanical properties of polyurethane networks based on poly(butadiene) diol, 4,4′-diphenylmethane diisocyanate (MDI) and poly(oxypropylene) triol (POPT) prepared at various initial ratios of reactive groups were studied. An inhomogeneous structure of the networks was revealed by small-angle X-ray scattering. The microdomains consist of POPT molecules crosslinked with MDI and they have a diameter of about 4–5 nm. The characteristic distance of microdomains is about 9 nm. The poor mutual miscibility of the reaction components and the existence of hydroxyl group association in the reaction mixture are the probable reasons for microdomain formation. The strain dependence of the equilibrium elastic force obeyed the Mooney–Rivlin equation. The experimental moduli of dry and equilibrium swollen samples were higher than those calculated for the affine limit of the Flory junction fluctuation model on the assumption of a homogeneous network formation.

(Keywords: polyurethane; network; inhomogeneity)

INTRODUCTION

Polymer networks represent an interesting subject of study for polymer chemistry and physics. The elastic equilibrium behaviour of many homogeneous as well as inhomogeneous networks in uniaxial extension is described well by the phenomenological Mooney–Rivlin equation[1,2]:

$$[f^*]=2C_1+2C_2\alpha^{-1} \tag{1}$$

where C_1 and C_2 are constants, $[f^*]\equiv fv_p^{1/3}/[A_d(\alpha-\alpha^{-2})]$ is the reduced stress, f is retractive force, v_p is volume fraction of the polymer in the equilibrium swollen network, A_d is cross-sectional area of the dry sample and α is the extension ratio defined by $\alpha\equiv L/L^\circ$, L and L° being the lengths of the sample in the deformed and undeformed state, respectively. This equation holds up to the high deformation region where an upturn of the stress–strain curve in the Mooney–Rivlin plot ($[f^*]$ *versus* α^{-1}) appears. The upturn can be caused, for example, by finite chain extensibility or strain-induced crystallinity[2].

There have been a number of attempts to build up an adequate microphysical theory of the elasticity of polymer networks. Although the entropic origin of the retractive force was proved long ago, owing to the complicated topology of networks and the presence of space constraints (entanglements) this problem has not yet been definitively solved. Individual theories differ mainly in the way by which they take into account these two network features.

The constraint junction fluctuation model of Flory and Erman[3] considers that entanglements influence the junction fluctuations only and predicts that the reduced stress of an ideal network (in which the defects like loops and free chain ends are not present) has to lie between phantom $[f^*_{ph}]$ and affine $[f^*_{aff}]$ moduli determined by the network connectivity:

$$\frac{\xi kT}{V^\circ}=[f^*_{ph}]\leqslant[f^*]\leqslant[f^*_{aff}]=\frac{\nu kT}{V^\circ} \tag{2}$$

where k is the Boltzmann constant, T is the absolute temperature and V° is the volume of the network in the undeformed state; ξ and ν are the cycle rank and the number of chains in the network, respectively. The cycle rank was first introduced by Flory[4]; it is the number of chains which have to be cut to reduce the network to a connected graph of acyclic structure (spanning tree).

In imperfect networks not all chains contribute to the elasticity. To be able to use equation (2) the problem arises of counting the number of chains participating in imperfect network elasticity. In this case, Scanlan[5] and Case[6] have suggested using the number of elastically active chains ν_a. An elastically active chain is defined as that terminated by two active junctions (junctions with at least three independent infinite continuations) at its ends.

It follows from the constrained junction fluctuation model that small-strain $(2C_1+2C_2)$ and large-strain $(2C_1)$ moduli of the Mooney–Rivlin equation should be near to the affine and phantom moduli, respectively. Because the intensity of interchain constraints decreases with swelling, the reduced stress of the highly swollen network is almost independent of strain and its value should be near to the phantom modulus, too.

* To whom correspondence should be addressed

0032-3861/93/163437-09

In other models[7–10] the influence of constraints affecting the conformation of the whole chain is counted and a certain 'entanglements' contribution to reduced stress is predicted.

To test predictions of microphysical theories of rubber elasticity, it is necessary to have a convenient material with well defined structure. The determination of the real structure of a network is the main source of controversy in the literature. Networks prepared by end-linking of prepolymer chains with narrow polydispersity by a proper crosslinking agent seem to be the most convenient for this purpose, but perfection of the structure is difficult to achieve.

The elastic properties of networks can be influenced significantly by the presence of inhomogeneity. It can be formed, for example, by adding filler particles, by segregation of 'hard' blocks or by an association of chains of a given length in bimodal networks.

Also, in swollen gels the microsyneresis leading, after a sudden change in temperature, to microphase separation of the diluent in the gel matrix affects the elastic behaviour[11–13]. These inhomogeneities were reflected by an increase in the $2C_2$ parameter.

The moduli of the carbon black or silica-filled networks are higher due to reinforcement effects[14]. Their elastic properties can be explained, for example, in terms of the two-phase Takayanagi model[15]. On the other hand, Mark and Andrady[16] observed that the moduli of inhomogeneous bimodal poly(dimethylsiloxane) networks prepared by two-stage end-linking of chains of two different lengths were not affected by the inhomogeneity and were equal to the moduli of corresponding homogeneous networks. In other words, no reinforcement effect caused by the heterogeneity in these networks was observed.

If the heterogeneities are large enough, they can be detected by light scattering (if they have a refractive index distinct from the rest of the material), by d.s.c. (if they differ in specific heat capacity and glass transition temperature) or by electron microscopy. If the heterogeneities differ in the electron density, it is possible to detect them by small-angle X-ray scattering (SAXS). Due to the small wavelength of X-rays, this method is rather sensitive and makes it possible to detect heterogeneities with a diameter of the order of nanometres.

The presence of inhomogeneous structure in segmented polyurethanes is well known. Studies have been made[17–19] of polybutadiene-based polyurethanes prepared using various diisocyanates and low-molecular diols as extenders. The conclusion was reached that phase separation during polymerization or as a consequence of incompatibility of the reactants was the probable reason for the formation of microdomains of various size.

In this paper, the (in)homogeneity of networks prepared from poly(butadiene) diol (PBD), 4,4'-diphenylmethane diisocyanate (MDI) and poly(oxypropylene) triol (POPT) and its influence on the resulting equilibrium mechanical properties of the networks were studied by SAXS, d.s.c. and a uniaxial extension test.

EXPERIMENTAL

Materials

The PBD (Research Institute for Synthetic Rubber, Kralupy n. Vlt., CSFR) used in the network preparation had a number average molecular weight, $\bar{M}_n = 5100$ g mol^{-1}, a narrow polydispersity, $\bar{M}_w/\bar{M}_n = 1.1$, microstructure of 62% vinyl-1,2, 24% *trans*-1,4, 14% *cis*-1,4 and number average functionality, $\bar{f}_n = 1.91$. POPT (Niax Polyols) had $\bar{M}_n = 710$ g mol^{-1} and $\bar{f}_n = 1.89$. The hydroxyl groups of PBD were mainly of primary type while those of POPT were secondary; their reactivities were different.

The functionality distributions of PBD, s_i, and POPT, t_i, were determined by g.p.c. and the number fractions of functionalities (see Appendix) were $s_0 = 0.010$, $s_1 = 0.101$, $s_2 = 0.889$ and $t_2 = 0.11$, $t_3 = 0.89$.

Networks were prepared by a one-stage process. The initial concentrations of reactive groups in samples used in this study varied as follows:

$$[OH]_{PBD}:[NCO]_{MDI}:[OH]_{POPT} = 1:2:r_{TD}$$

where r_{TD} are the initial concentrations of the triol hydroxyls (for samples 1–5 $r_{TD} = 1.00$, 1.15, 1.30, 1.40 and 1.50, respectively). After 15 min mixing in a nitrogen atmosphere at 60°C, 0.001 wt% catalyst (dibutyltin dilaurate) was added and the reaction mixtures were poured into a Teflon mould of rectangular shape. The reaction proceeded at 70°C for 24 h. The prepared samples were in the form of sheets about 1 mm in thickness.

To determine the mass fraction of sol, pieces of the samples were extracted in benzene or chloroform at 25°C for 3 weeks, then dried to constant weight. The mass fraction of sol was calculated from the decrease in mass.

For swelling experiments bis(2-methoxyethyl) ether (diglyme) was used.

For scattering experiments, the following mixtures were prepared: PBD + MDI($[OH]_{PBD}:[NCO]_{MDI} = 1:2$), PBD + POPT($[OH]_{PBD}:[OH]_{POPT} = 1:1$) and PBD + MDI + POPT($[OH]_{PBD}:[NCO]_{MDI}:[OH]_{POPT} = 1:2:1$). The components were mixed intensively for 15 min at 60°C without using a catalyst. All mixtures were liquid.

Small-angle X-ray scattering

SAXS curves were measured with a Kratky camera using CuKα radiation with wavelength, $\lambda = 0.1542$ nm. Intensities were transformed to smeared differential scattering cross-section (absolute scale) $d\tilde{\Sigma}/d\Omega(q)$ using the Lupolen sample as a secondary standard[20] and relation:

$$\frac{d\tilde{\Sigma}}{d\Omega}(q) = \frac{a}{\tilde{I}_L K_L T h}\tilde{I}(q)$$

where $\tilde{I}(q)$ is the measured intensity, $q = 4\pi/\lambda \sin\Theta$ is the magnitude of the scattering vector, 2Θ is the scattering angle, a is the sample–detector distance, T and h are transmission and thickness of the sample, respectively, K_L is the calibration constant and $\tilde{I}_L$ is the intensity of radiation scattered by the standard for $q = 2\pi/(15\text{ nm})$.

The differential scattering cross-section, $d\Sigma/d\Omega(q)$, was calculated by the program DESMGLAT[21], which is based on the transformation:

$$\frac{d\tilde{\Sigma}}{d\Omega}(q) = \frac{2}{K}\int_{-\infty}^{\infty}\int_{0}^{\infty} Q(x)P(t)\frac{d\Sigma}{d\Omega}[\sqrt{(q-x)^2+t^2}]\,dx\,dt$$

where $K = 2\pi/a\lambda$ and $P(t)$, $Q(x)$ describe the distribution of intensity along the primary beam length and width, respectively. The primary beam profiles are normalized so that $P(0) = 1$ and $\int_{-\infty}^{\infty} Q(x)\,dx = 1$.

The mean square scattering density fluctuation $(\overline{\Delta\rho})^2$, which is a measure of sample heterogeneity, was obtained according to the equation[22,23]:

$$(\overline{\Delta\rho})^2 = \frac{K}{4\pi^2}\int_0^\infty q\frac{d\tilde{\Sigma}}{d\Omega}(q)\,dq \tag{3}$$

The characteristic distance of heterogeneities D (which corresponds approximately to the 'average' distance of their centres) was calculated from the Bragg equation:

$$D = \frac{2\pi}{q_{max}} \tag{4}$$

where q_{max} is the magnitude of the scattering vector at maximum intensity.

The specific inner surface was calculated from the equation[22]:

$$\frac{S}{V} = \pi v_1 v_2 \frac{\lim_{q\to\infty} q^3\frac{d\tilde{\Sigma}}{d\Omega}(q)}{\int_0^\infty q\frac{d\tilde{\Sigma}}{d\Omega}(q)\,dq} \tag{5}$$

where v_1, v_2 are the volume fractions of phases.

Uniaxial extension measurements

For mechanical experiments, rectangular specimens of about 4 cm in length were cut. Their cross-sectional area ($\sim 1 \times 4$ mm^2) was measured by a travelling microscope. The samples were mounted in clamps about 3 cm apart; the upper clamp was attached to a force transducer (Hottinger Baldwin Messtechnik) kept at a constant temperature of 37°C. The force transducer was calibrated twice, before and after the experiment, and the calibration confirmed that the relation between stress and output voltage was linear throughout the experimental range used. The output voltage was recorded using a plotter.

Stress–strain studies were carried out by a multistep relaxation experiment. Measurements were performed in a temperature-controlled chamber (30°C). To determine the extension ratios, two fine reference marks were made on the specimens using white ink at a distance of about 1.5 cm apart; the distance was measured by a cathetometer (accuracy of 0.01 mm). The elongation was increased stepwise and the sample was allowed to relax for about 30 min. The time dependence of stress was recorded. The equilibrium stress $\sigma_e(\alpha)$ was then obtained by extrapolation of the measured stress $\sigma(\alpha, t)$ to infinite time using the Chasset–Thirion equation[24]:

$$\sigma(\alpha, t) = \sigma_e(\alpha)[1 + (t/\tau)^{-m}]$$

where t is the time of relaxation and $\tau, m > 0$ are parameters. The validity of the stress superposition and independence of the relaxation on the extension ratio were assumed. The values of the parameters of the Chassett–Thirion equation were established in advance, in a series of long-time relaxations.

However, the question arises of whether the equilibrium values of stress calculated by the extrapolation are sufficiently reliable. At least, the quicker the relaxation, the more reliable are the extrapolated values.

Equilibrium swollen samples in diglyme were also measured at 30°C. In this case the extrapolation was not necessary as the relaxation was fairly rapid.

I.r. and d.s.c.

The conversion of NCO groups in networks was determined by infrared spectroscopy (band at 2300 cm^{-1}) on a Perkin–Elmer 580B.

The d.s.c. measurements of networks were performed on a Perkin–Elmer DSC-2 (−60 to 0°C) and a Perkin–Elmer DSC-6 (0–250°C). The heating rate was 10°C min^{-1} in both cases.

RESULTS AND DISCUSSION

Structure of networks

All samples were transparent and their d.s.c. thermograms (*Figures 1* and *2*) did not show any presence of a

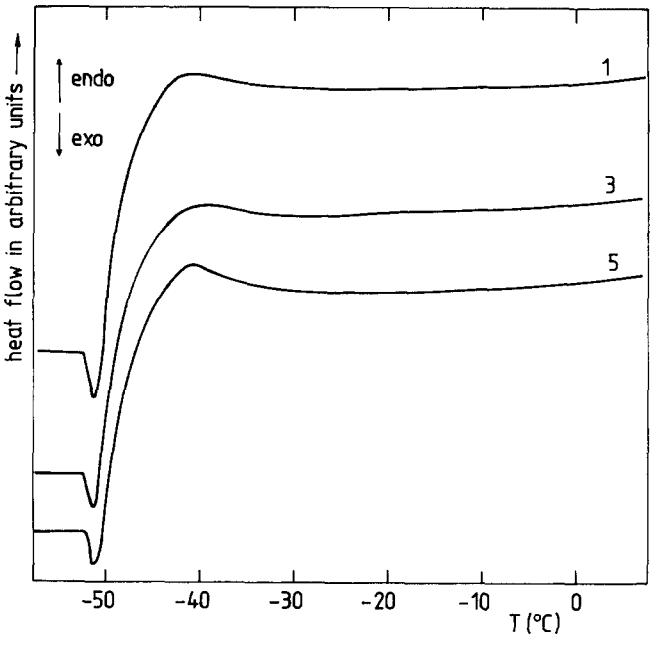

Figure 1 D.s.c. diagrams of networks at −60 to 0°C. The numbers indicate the measured networks (see *Table 1*)

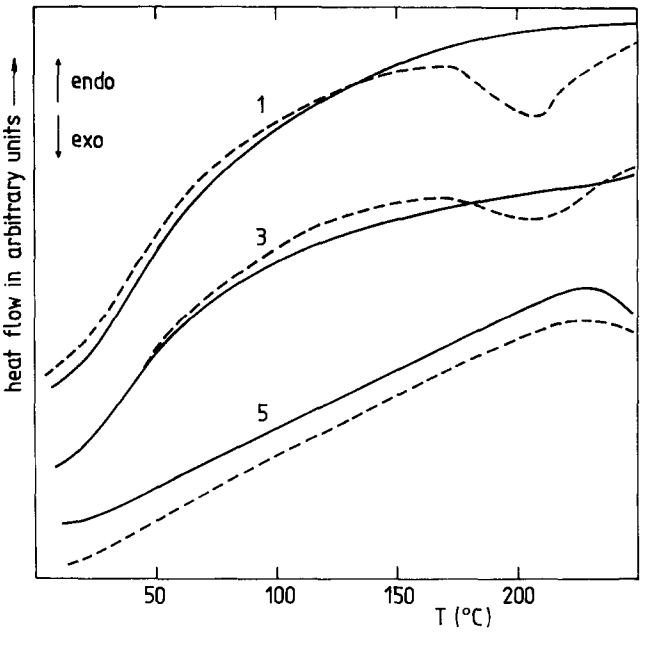

Figure 2 D.s.c. diagrams of networks at 0–250°C; ----, first run; ——, second run

two-phase structure. Exotherms at about 180°C are caused by thermal instability of networks at higher temperatures.

In spite of that, SAXS revealed a fine heterogeneity of all networks (*Figure 3*). On all scattering curves, one can see distinct maxima (even for network no. 1 swollen to equilibrium in diglyme). From the scattering curves, the mean square scattering density fluctuations, characteristic distances between heterogeneous regions and specific inner surface were calculated (*Table 1*, from equations (3)–(5)).

The characteristic distance of heterogeneities in dry networks is about 8–9 nm. In network no. 1 it is about 13 nm ($q_{max} = 0.49\ nm^{-1}$, *Figure 3*), which is in accordance with an increase in distance with degree of swelling.

The results of scattering experiments on PBD and PBD + MDI, PBD + POPT, PBD + MDI + POPT mixtures are given in *Figure 4*. The cross-section* for PBD is about $0.02\ cm^{-1}$ and it is approximately constant.

* The values of the cross-section for very small q values are not very exact due to the necessity for collimation corrections

Its limiting value for $q \to 0$ is connected with the isothermal compressibility κ_T and scattering density ρ by the equation[25]:

$$\lim_{q \to 0} \frac{d\Sigma}{d\Omega}(q) = kT\kappa_T\rho^2$$

and it corresponds to a compressibility of about $830\ MPa^{-1}$. Unfortunately, we were not able to compare this value with the experimental one. In spite of considerable uncertainty of scattering data in the region of small q values it can be concluded that the isothermal compressibility of the unreacted mixture of PBD + MDI + POPT is much higher than the compressibility of the network of the same composition, as could be expected.

The scattering curves for PBD + MDI and PBD + POPT mixtures are similar, without distinct minima or maxima. However, on the scattering curve for PBD + MDI + POPT mixture (of the same composition as network no. 1) there is a maximum at $q \approx 0.7\ nm^{-1}$, which corresponds

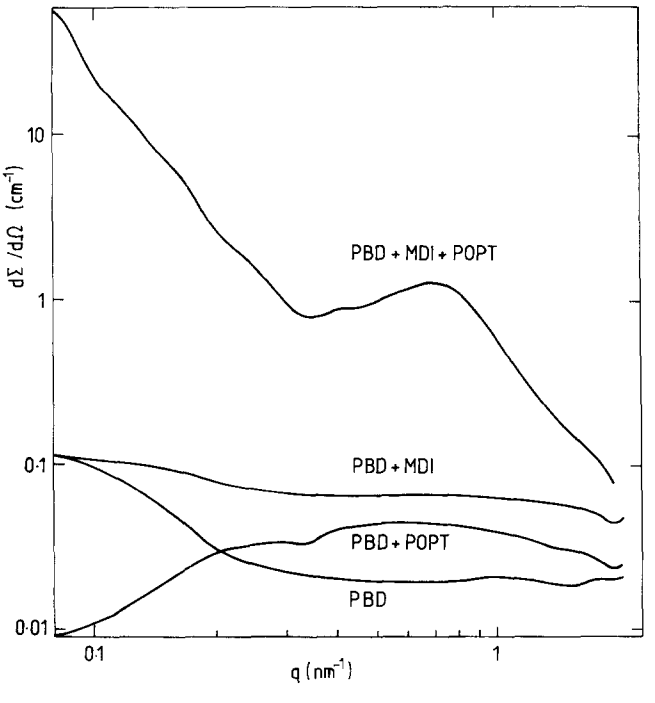

Figure 3 Plot of the scattering cross-section $d\Sigma/d\Omega$ *versus* magnitude of the scattering vector q for mixtures

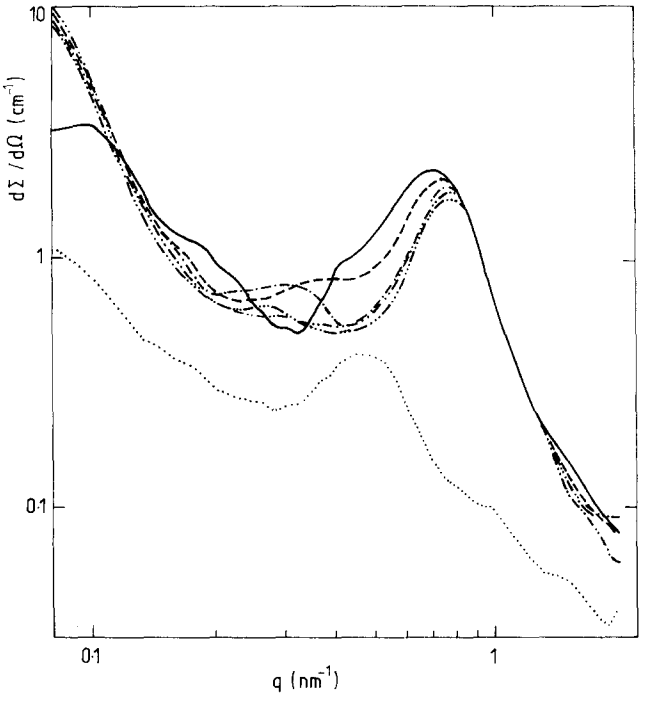

Figure 4 Plot of the scattering cross-section $d\Sigma/d\Omega$ *versus* magnitude of the scattering vector q for networks (see *Table 1*): (——, network no. 1; – – –, no. 2; –·–·–, no. 3; –··–··–, no. 4; ····, equilibrium swollen network no. 1 (in diglyme)

Table 1 Scattering data (q_{max} is the value of the scattering vector corresponding to the maximum of intensity, D is the characteristic distance, d is the specific mass at 30°C, $\overline{(\Delta\rho)^2}$(exp) and (calc) are the experimental and calculated mean square scattering density fluctuation, respectively, S/V is the specific inner surface)

No.	q_{max} (nm^{-1})	D (nm)	d ($g\ cm^{-3}$)	$\overline{(\Delta\rho)^2} \times 10^{-20}$ (exp) (cm^{-4})	$\overline{(\Delta\rho)^2} \times 10^{-20}$ (calc) (cm^{-4})	S/V (nm^{-1})
1	0.67	9.4	0.9336	0.53	0.73	1.66
2	0.72	8.7	0.9354	0.52	0.74	1.69
3	0.76	8.3	0.9358	0.48	0.70	1.76
4	0.77	8.2	0.9365	0.40	0.69	1.71
5	0.77	8.2	0.9375	0.46	0.69	1.74

to the characteristic distance of 9 nm. Therefore an inhomogeneous structure is also present in unreacted mixtures of PBD, MDI and POPT.

The component with higher specific mass and electron density is MDI. To give high values of cross-sections and maxima in scattering experiments, MDI molecules must be spatially concentrated in certain regions. Further, the conversion of NCO groups was high ($\geqslant$99.5%) in all samples. So, MDI molecules must be joined by (relatively small) POPT molecules. Microdomains of this structure are then joined by means of long PBD chains* (*Figure 5*).

If we suppose this precise network structure, it is possible to calculate the specific masses and volume fractions of microdomains in samples from the densities of samples and the density of PBD, and to calculate the mean square scattering density fluctuation from the following equation[26]:

$$(\overline{\Delta\rho})^2 = v_1 v_2 (\rho_1 - \rho_2)^2 \quad (6)$$

where v_1, v_2 are volume fractions of PBD and microdomains, respectively.

This equation holds precisely only for sharp interphase boundaries, i.e. for microdomains of larger size. The volume fraction of PBD changes from 0.88 to 0.85 (nos 1–5). The scattering density of the material ρ is given by:

$$\rho = \frac{\sum_i Z_i}{\sum_i M_i} N_A b d$$

where Z_i and M_i are atomic number and relative atomic mass of the material, respectively, $b = 2.82 \times 10^{-15}$ m is the scattering amplitude for one electron according to Thomson's formula, N_A is the Avogadro constant and d is the specific mass of the material.

The calculated values of the mean square scattering density fluctuation are given in *Table 1*. For dry samples, they are all higher than the experimental values. This is caused mainly by the too-idealized assumption of complete phase separation in the system and by the non-sharp interphase boundary of microdomains. Assuming a uniform size and spherical shape of all microdomains, their radius R is:

$$R = \frac{D}{2}\left(\frac{3v_2\sqrt{2}}{\pi}\right)^{(1/3)} = 2.4\text{–}2.6 \text{ nm}$$

The size calculated from the specific inner surface (*Table 1*) is:

$$R = \frac{3}{v_1(S/V)} \approx 2 \text{ nm}$$

The sphere of this radius may contain only a few hundred molecules (MDI and POPT) and it is subjected to large relative fluctuations of its form and size. The segments of microdomain wander for small distances into the BPD matrix which is expressed by a diffuse interphase boundary. Therefore the expected experimental values of the mean square scattering density fluctuation should be lower than the values calculated on the assumption of a sharp boundary (*Table 1*).

The most probable reason for the formation of microdomains is the poor mutual miscibility of the reaction components (PBD, MDI and POPT). There is a large difference in solubility parameters between PBD, POPT and MDI (see *Table 2*) and therefore a

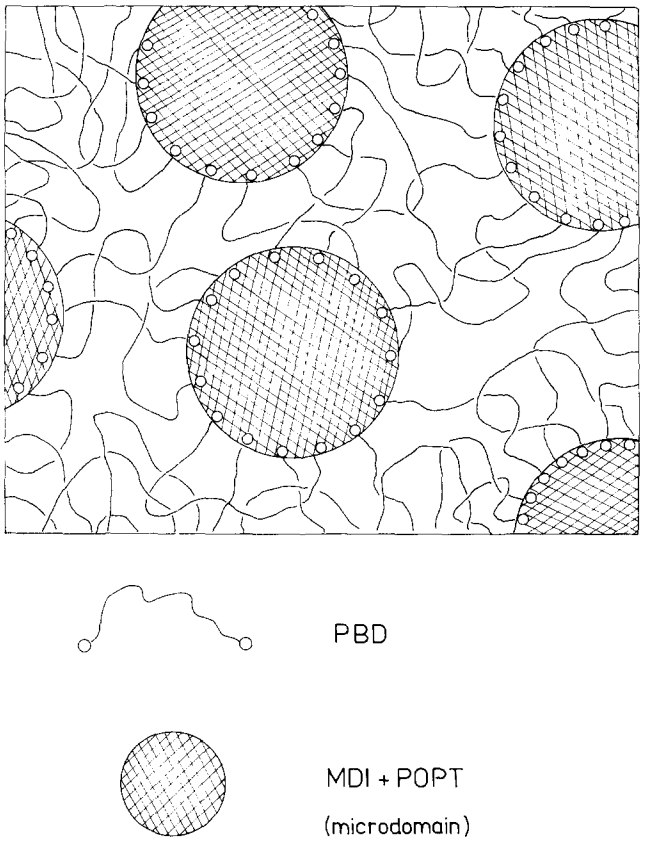

Figure 5 Schematic diagram of the inhomogeneous structure of networks

* The root mean square end-to-end distance of PBD chains calculated on the assumption of the additivity of the contributions to the characteristic ratio from 1,2- and 1,4-components is about 6 nm. It is sufficient to connect the microdomains

Table 2 Some parameters of the reaction components (d is the specific mass at 30°C, $\bar{M}_n$ is the number-average molecular weight, M_r is the segment molecular weight, V_r is the segment molar reference volume, N is the number of segments, δ is the solubility parameter at 25°C)

	d (g cm^{-3})	$\bar{M}_n$ (g mol^{-1})	M_r (g mol^{-1})	V_r (cm^3 mol^{-1})	N	δ (cal$^{1/2}$ cm$^{-3/2}$)
PBD	0.897	5200	54	60	96	8.5[a]
MDI	1.19[b]	250	–	60	4	9.8[c]
POPT	0.924	708	58	63	12	8.6[d]

[a] Value for amorphous poly(butadiene) with 82% 1, 2– (ref. 32)
[b] At liquid state at 50°C
[c] Ref. 33
[d] Value for poly(oxypropylene)[33]

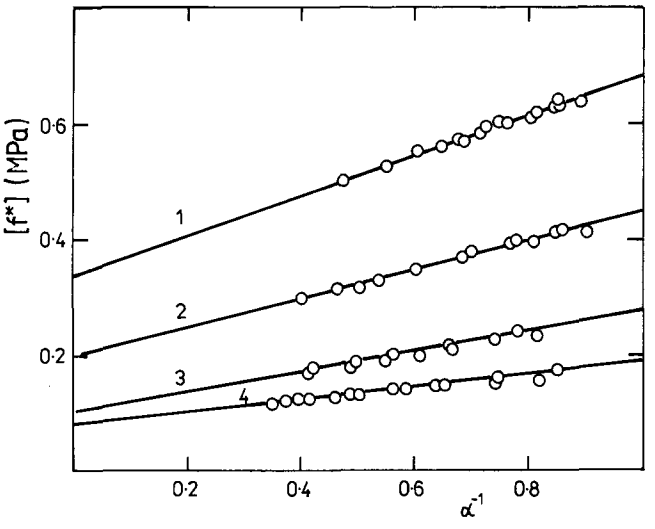

Figure 6 Mooney–Rivlin plot for dry networks. [f^*] is the reduced stress, α is the extension ratio; the numbers indicate the measured networks (see *Table 1*)

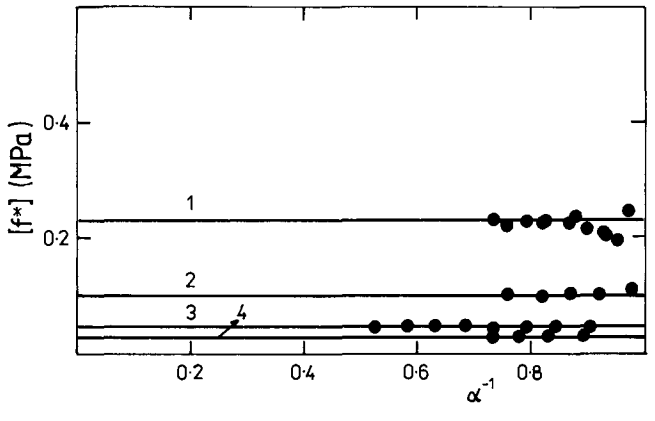

Figure 7 Mooney–Rivlin plot for equilibrium swollen networks (in diglyme)

phase separation can be expected for this system. SAXS experiments on unreacted mixture confirm this conclusion.

This tendency is further supported by the formation of associates of the polar hydroxyl groups through hydrogen bonds in the non-polar environment of polybutadiene chains. The existence of such associates, even at higher temperatures and in the presence of a non-polar solvent, has been confirmed by measurements of the temperature dependence of the dynamic viscosity for the PBD and the acetylated PBD[27].

In this context, it is interesting to compare the obtained results with those of Williams *et al.*[28]. They studied ionic aggregation using carboxyl-terminated polybutadienes and polyisoprenes as model ionomers. These telechelic polymers were stoichiometrically neutralized by various metal alkoxides by which aggregates of higher electron density were formed. For carboxyl-terminated polybutadiene*, the authors found that aggregates with a diameter of about 0.6–0.9 nm had the characteristic distance of about 6–7 nm. They observed that the distance between the surfaces of the aggregates was approximately the same (~4–5 nm) and did not depend on the nature of the ion. It was of the same order as the root mean square end-to-end distance of 7 nm.

Elastic behaviour

The stress–strain characteristics are given in *Figure 6*. They demonstrate that all samples obey the Mooney–Rivlin equation well. The characteristics of sample no. 5 were not calculated due to a very slow relaxation and unreliable extrapolation of the measured values to the equilibrium values. The reduced stress of equilibrium swollen samples is independent of strain (*Figure 7*). The values of Mooney–Rivlin parameters and of moduli of swollen samples were then calculated by linear regression (*Figure 8*).

The values calculated on the assumption of homogeneous end-linking are also given in *Figure 8*. Both experimental values of small-strain $2C_1+2C_2$ and large-strain $2C_1$ limits are much higher than the calculated values of affine and phantom moduli, respectively. The values of $2C_1$ are higher than the corresponding moduli of equilibrium swollen samples and also exceed the calculated phantom moduli. For a homogeneous network, such a high value would correspond to a high entanglement contribution to the elasticity. In an inhomogeneous network, the influence of excluded volume (of microdomains) on conformations of PBD chains or a filler effect of microdomains could be possible reasons for higher moduli.

Due to the different (but unknown) reactivity of the secondary (triol) and primary (diol) hydroxyl groups, the ratio of the rate constants of the respective hydroxyl

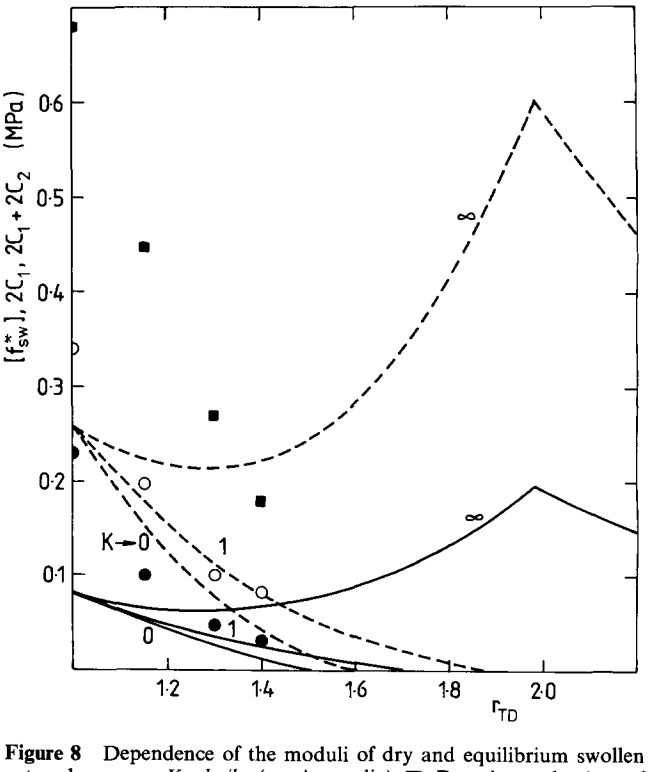

Figure 8 Dependence of the moduli of dry and equilibrium swollen networks on r_{TD}, $K=k_T/k_D$ (see Appendix). ■, Experimental values of small deformation modulus ($2C_1+2C_2$); ○, experimental values of high deformation modulus ($2C_1$); ●, experimental values of equilibrium modulus of equilibrium swollen networks ([f^*_{sw}]); ——, calculated dependence of [f^*_{ph}]; – – –, calculated dependence of [f^*_{aff}]

* $\bar{M}_n=4600\ g\ mol^{-1}$, $\bar{M}_w/\bar{M}_n=1.8$, microstructure 4% vinyl-1,2, 71% *trans*-1,4, 25% *cis*-1,4

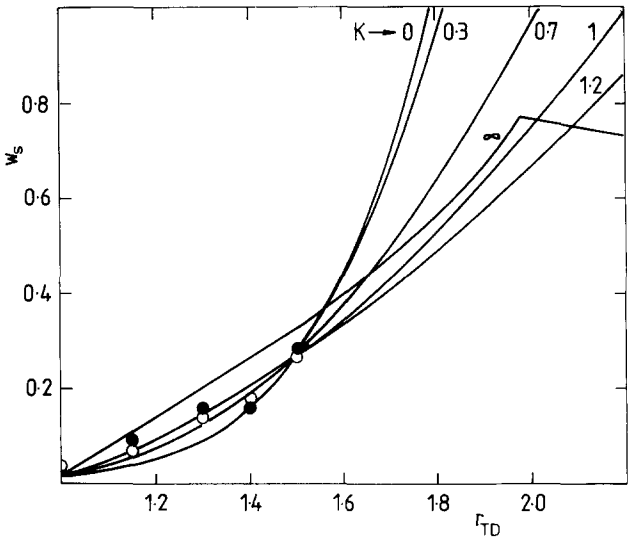

Figure 9 Dependence of mass fraction of sol w_S on r_{TD} assuming homogeneous network formation; $K \equiv k_T/k_D$ is the ratio of the rate constants of triol to diol hydroxyls (see Appendix). ——, Calculated values; ●, extraction in benzene; ○, extraction in chloroform

groups with MDI, K, (cf. Appendix) was used for the characterization of their relative reactivity. The limits are given by the extreme values of the K parameter. The values of the mass fraction of sol (*Figure 9*) for all samples lie between the calculated limits ($K \to 0$ and ∞, respectively). The value $K \approx 1.2$, which corresponds to a somewhat higher reactivity of the POPT hydroxyls, offers the best fit of the experimental values.

CONCLUSIONS

Small-angle X-ray scattering revealed that networks prepared from PBD, MDI and POPT have an inhomogeneous structure with characteristic microdomain distance of about 8–9 nm. One phase (of lower electron density) consists of non-polar polybutadiene chains, while the other phase consists of polar POPT molecules crosslinked with MDI. This assumption about the structure implies that the microdomain diameter is about 5 nm and the distance between their surfaces is about 3–4 nm. Therefore, the length of PBD chains ($\sqrt{\langle r^2 \rangle_0} \approx 6$ nm) is sufficient for mutual connection of microdomains.

Microdomains are too small to be identified by other less sensitive methods such as d.s.c. or light scattering. However, their presence can significantly influence mechanical properties of networks. A probable reason for their formation is a poor miscibility of polar and non-polar components of the system. The association of polar hydroxyl groups by hydrogen bonds in a non-polar medium of polybutadiene chains may also be very important. Both factors lead to an inhomogeneous distribution of the reactive groups in the reaction volume and thus to inhomogeneous crosslinking.

The equilibrium elastic measurements of samples demonstrated their highly elastic properties which can be described well by the phenomenological Mooney–Rivlin equation. Experimentally established moduli (low, high deformation and moduli of equilibrium swollen samples) of networks closer to stoichiometry are higher than the corresponding theoretical values determined by the number of chemical crosslinks in networks according to the constrained junction model.

REFERENCES

1 Rivlin, R. S. and Saunders, D. W. *Phil. Trans. R. Soc. London* 1951, **A243**, 251
2 Treloar, L. R. G. 'The Physics of Rubber Elasticity', 3rd Edn, Clarendon Press, Oxford, 1975
3 Flory, P. J. and Erman, B. *Macromolecules* 1982, **15**, 800
4 Flory, P. J. *Proc. R. Soc. London* 1976, **A351**, 351
5 Scanlan, J. *J. Polym. Sci.* 1960, **43**, 501
6 Case, L. C. *J. Polym. Sci.* 1960, **45**, 397
7 Edwards, S. F. *Proc. Phys. Soc.* 1967, **91**, 513
8 Gaylord, R. J. *Polym. Eng. Sci.* 1979, **19**, 263
9 Heinrich, G., Straube, E. and Helmis, G. *Adv. Polym. Sci.* 1988, **85**, 33
10 Edwards, S. F. and Vilgis, T. A. *Rep. Prog. Phys.* 1988, **51**, 243
11 Ilavský, M. and Prins, W. *Macromolecules* 1970, **3**, 415, 425
12 Ilavský, M. and Dušek, K. *J. Polym. Sci., Polym. Symp. Edn* 1975, **53**, 257
13 Ilavský, M., Hrouz, J. and Dušek, K. *J. Macromol. Sci.-Phys.* 1981, **B19**, 227
14 Mark, J. E. and Erman, B. 'Rubber-like Elasticity. A Molecular Primer', Wiley Interscience, New York, 1988
15 Takayanagi, M., Uemura, S. and Minami, S. *J. Polym. Sci.* 1963, **C5**, 113
16 Mark, J. E. and Andrady, A. L. *Rubber Chem. Technol.* 1981, **54**, 366
17 Xu, M., MacKnight, W. J., Chen, C. H. Y. and Thomas, E. L. *Polymer* 1983, **24**, 1327
18 Bengtson, B., Feger, C., MacKnight, W. J. and Schneider, N. S. *Polymer* 1985, **26**, 895
19 Li, C., Goodman, S. L., Albrecht, R. M. and Cooper, S. L. *Macromolecules* 1988, **21**, 2367
20 Kratzky, O., Pilz, J. and Schmidt, P. J. *J. Colloid Interface Sci.* 1966, **61**, 24
21 Glatter, O. *J. Appl. Cryst.* 1974, **7**, 147
22 Kratky, O. *Prog. Biophys.* 1963, **13**, 105
23 Pleštil, J. and Hlavatá, D. *Polymer* 1988, **29**, 2216
24 Chasset, R. and Thirion, P. *Chim. Ind. (Paris)* 1967, **97**, 617
25 Uhlmann, D. R., Renninger, A. L., Kritchevsky, G. and Vander Sande, J. *J. Macromol. Sci.-Phys.* 1976, **B12**, 153
26 Alexander, L. E. 'X-Ray Diffraction Methods in Polymer Science', R. E. Krieger, New York, 1979
27 Ghafari, M. E. and Pham, Q. T. *Makromol. Chem.* 1983, **184**, 1669
28 Williams, C. E., Russell, T. P., Jérôme, R. and Horrion, J. *Macromolecules* 1986, **19**, 2877
29 Dobson, G. R. and Gordon, M. *J. Chem. Phys.* 1965, **43**, 705
30 Dušek, K. *Adv. Polym. Sci.* 1986, **78**, 1
31 Krakovský, I., Havránek, A., Ilavský, M. and Dušek, K. *Colloid Polym. Sci.* 1988, **266**, 324
32 Yakashita, S., Minoura, Y. and Maekawa, E. *Makromol. Chem.* 1979, **180**, 705
33 Nishimura, H., Kojima, H., Yarita, T. and Noshiro, M. *Polym. Eng. Sci.* 1986, **26**, 585

APPENDIX

Calculation of the structural parameters of networks on the assumption of homogeneous crosslinking using the theory of branching processes

To discuss the influence of heterogeneity on elastic properties of the studied networks, the structural parameters of the corresponding homogeneous networks have been calculated. In the calculation given below, cyclization has been neglected, but the functionality distributions of PBD and POPT have been considered. The post-gel stage is addressed exclusively.

The components presented in our system are represented schematically in *Figure 10*. The functionality distributions of 0, 1, 2 and 2, 3 functional components in PBD and POPT are described by number fractions s_0, s_1, s_2 and t_2, t_3, respectively. We suppose that in our system the

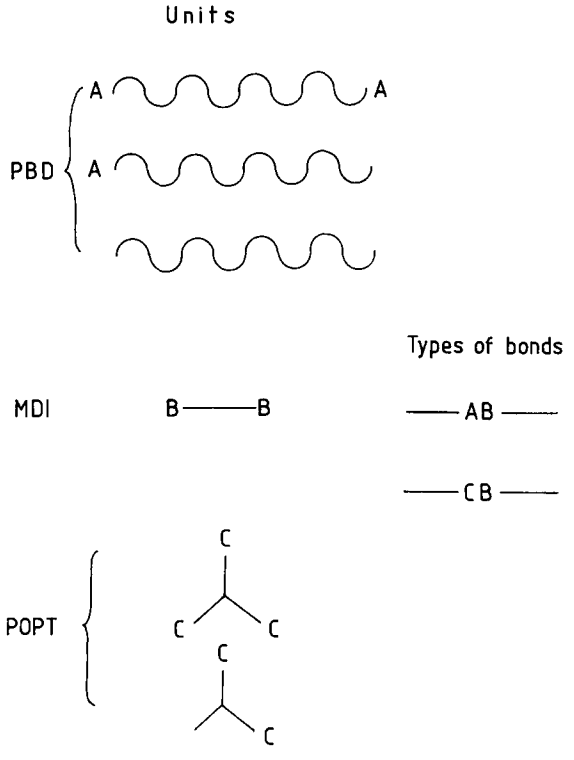

Figure 10 Representation of the system in the theory of branching processes. Functional groups: A, primary (diol) hydroxyls; B, isocyanate groups; C, secondary (triol) hydroxyls

reactions:

$$A+B\rightarrow AB$$
$$C+B\rightarrow CB$$

are possible.

The key role in calculations of network structure is played by the extinction probabilities of the oriented chemical bonds which join the reactive molecules. The orientation of a bond IJ means that this bond originates in group I of a molecule and goes directly to group J of another molecule which is joined to the former one. The extinction probability for the oriented bond IJ is defined as the probability that the bond has finite continuation only[29].

In our case there are four kinds of oriented bonds:

$$A\rightarrow B \qquad B\rightarrow A$$
$$C\rightarrow B \qquad B\rightarrow C$$

and by the well-known procedure (see, for example, refs 30 or 31), it is possible to derive the following equations for extinction probabilites:

$$v_{BA}=(2s_2V_{AB}+s_1)/(2s_2+s_1)$$
$$v_{BC}=(3t_3V_{CB}+2t_2)/(3t_3+2t_2)$$
$$v_{AB}=v_{CB}=(V_{BA}+V_{BC}-1)$$

where

$$V_{IJ}\equiv 1-\alpha_{IJ}+\alpha_{IJ}v_{IJ}$$

and α_{IJ} are the conversions of corresponding functional groups.

From stoichiometry we have two balance conditions:

$$2n_{MDI}\alpha_{BA}=(2s_2+s_1)n_{PBD}\alpha_{AB}$$
$$2n_{MDI}\alpha_{BC}=(3t_3+2t_2)n_{POPT}\alpha_{CB}$$

where n_{PBD}, n_{MDI}, n_{POPT} are the initial number fractions of species in the system.

If all components of functional distribution for PBD and POPT have the same molecular weight, the mass fraction of sol is given by the material with bonds of finite continuation only:

$$w_S=m_{PBD}(s_2V_{AB}^2+s_1V_{AB}+s_0)+m_{MDI}(V_{BA}+V_{BC}-1)^2+m_{POPT}V_{CB}^2(t_3V_{CB}+t_2)$$

where m_{PBD}, m_{MDI}, m_{POPT} are initial mass fractions in the system.

The number of elastically active junctions in the system is given by the number of units (see *Figure 10*) with at least three bonds with infinite continuation:

$$\mu_a=Nn_{POPT}t_3\alpha_{CB}^3(1-v_{CB})^3$$

where N is the number of units in the system, given by:

$$N=V^\circ d_{network}/\overline{M_n^\circ}$$

where $d_{network}$ is the specific mass of the network and V° the volume of network (in undeformed state of formation).

The number of elastically active chains is simply:

$$\nu_a=\tfrac{3}{2}\mu_a$$

and the cycle rank:

$$\xi=\nu_a-\mu_a=\tfrac{1}{2}\mu_a$$

Phantom and affine moduli are given by equation (2).

Mass fractions of species are related to number fractions as:

$$m_{PBD}=n_{PBD}M_{PBD}/\overline{M_n^\circ}$$
$$m_{MDI}=n_{MDI}M_{MDI}/\overline{M_n^\circ}$$
$$m_{POPT}=n_{POPT}M_{POPT}/\overline{M_n^\circ}$$

where $\overline{M_n^\circ}=n_{PBD}M_{PBD}+n_{MDI}M_{MDI}+n_{POPT}M_{POPT}$ is the initial number average molecular weight of the system and M_{PBD}, M_{MDI}, M_{POPT} are the respective molecular weights.

The conversions of groups remain to be established; they are determined by the kinetics. Let us assume that the reaction rates are described by the following differential equations for the concentrations:

$$-\mathrm{d}[A]/\mathrm{d}t=\mathrm{d}[AB]/\mathrm{d}t=k_D[A][B]$$
$$-\mathrm{d}[C]/\mathrm{d}t=\mathrm{d}[CB]/\mathrm{d}t=k_T[C][B]$$
$$-\mathrm{d}[B]/\mathrm{d}t=[B](k_D[A]+k_T[C])$$

where k_D, k_T are the rate constants for diol and triol hydroxyls with MDI, respectively. Initial concentrations are:

$$[A]_0=1$$
$$[B]_0=2$$
$$[C]_0=r_{TD}$$
$$[AB]_0=0$$
$$[CB]_0=0$$

It is better to seek the solutions as functions of $[A]$; the differential equations are transformed into the form:

$$\mathrm{d}[B]/\mathrm{d}[A]=1+K[C]/[A]$$
$$\mathrm{d}[C]/\mathrm{d}[A]=K[C]/[A]$$

$$d[AB]/d[A] = -1$$

$$d[CB]/d[A] = -K[C]/[A]$$

where $K \equiv k_T/k_D$ is the ratio of the rate constants and the conversions are:

$$\alpha_{AB} = [AB]/[A]_0$$

$$\alpha_{BA} = [AB]/[B]_0$$

$$\alpha_{BC} = [CB]/[B]_0$$

$$\alpha_{CB} = [CB]/[C]_0$$

The conversions as the solutions of the above differential equations are:

$$\alpha_{AB} = 1 - x$$

$$\alpha_{BA} = (1 - x)/2$$

$$\alpha_{BC} = r_{TD}(1 - x^K)/2$$

$$\alpha_{CB} = 1 - x^K$$

where

$$x \equiv [A]/[A_0]$$

The total conversion of NCO is:

$$\alpha_{BA} + \alpha_{BC} = \alpha_{NCO}$$

which gives a non-linear equation for x:

$$r_{TD}x^K + x - (2\alpha_{NCO} - r_{TD} - 1) = 0$$